MTOpen

original article

Embedding siRNA sequences targeting Apolipoprotein B100 in shRNA and miRNA scaffolds results in differential processing and *in vivo* efficacy

Piotr Maczuga[1,2], Jacek Lubelski[1], Richard van Logtenstein[1], Florie Borel[1,3], Bas Blits[1], Erwin Fakkert[4], Adalberto Costessi[4], Derek Butler[4], Sander van Deventer[2], Harald Petry[1], Annemart Koornneef[1] and Pavlina Konstantinova[1]

[1]Department of Research & Development, uniQure biopharma b.v., Amsterdam, The Netherlands; [2]Department of Gastroenterology and Hepatology, Leiden University Medical Center, Leiden, The Netherlands; [3]Department of Gastroenterology and Hepatology, Academic Medical Center, Amsterdam, The Netherlands; [4]Department of Genome Analysis, BaseClear b.v., Leiden, The Netherlands.

Overexpression of short hairpin RNA (shRNA) often causes cytotoxicity and using microRNA (miRNA) scaffolds can circumvent this problem. In this study, identically predicted small interfering RNA (siRNA) sequences targeting apolipoprotein B100 (siApoB) were embedded in shRNA (shApoB) or miRNA (miApoB) scaffolds and a direct comparison of the processing and long-term *in vivo* efficacy was performed. Next generation sequencing of small RNAs originating from shApoB- or miApoB-transfected cells revealed substantial differences in processing, resulting in different siApoB length, 5′ and 3′ cleavage sites and abundance of the guide or passenger strands. Murine liver transduction with adeno-associated virus (AAV) vectors expressing shApoB or miApoB resulted in high levels of siApoB expression associated with strong decrease of plasma ApoB protein and cholesterol. Expression of miApoB from the liver-specific LP1 promoter was restricted to the liver, while the H1 promoter-expressed shApoB was ectopically present. Delivery of 1×10^{11} genome copies AAV-shApoB or AAV-miApoB led to a gradual loss of ApoB and plasma cholesterol inhibition, which was circumvented by delivering a 20-fold lower vector dose. In conclusion, incorporating identical siRNA sequences in shRNA or miRNA scaffolds results in differential processing patterns and *in vivo* efficacy that may have serious consequences for future RNAi-based therapeutics.

Received 19 September 2011; accepted 11 July 2012; advance online publication 23 October 2012. doi:10.1038/mt.2012.160

INTRODUCTION

RNA interference (RNAi) is an evolutionary conserved mechanism for post-transcriptional regulation of gene expression. It plays an important role in defense against viruses but also in development and in normal functioning of the cell.[1,2] Since its discovery RNAi has become a valuable research tool for functional analysis of gene expression and a promising therapeutic approach for treatment of many disorders by silencing disease-related genes.[3] Significant progress has been made toward improving the specificity of RNAi-mediated target inhibition and minimizing its potential side-effects, yet more insight is needed on the exact small interfering RNA (siRNA) processing pattern when identical predicted sequences are incorporated in a short-hairpin RNA (shRNA) or artificial microRNA (miRNA) scaffold for therapeutic applications.

Processing of miRNA by RNAse III family endonucleases plays a central role in their proper functioning in the cell.[4] In the nucleus, Drosha cleaves primary miRNA precursors (pri-miRNAs) to produce ~70 nucleotides (nt) miRNA precursors (pre-miRNAs) with 2 nt 3′ overhang.[5] Pre-miRNAs are transported by Exportin 5 to the cytoplasm where Dicer, another member of the RNAse III endonuclease family produces a mature miRNA duplex of ~21–28 nt basepairs (bp).[6] Dicer also recognizes and processes shRNAs, which resemble the pre-miRNA structure. shRNAs with 19 bp or shorter stem may also be processed independently from Dicer cleavage, however the detailed mechanism has not been described.[7–9] The ~21–28 nt cleavage products enter a multiprotein RNA-induced silencing complex where one of the strands is used for the sequence-specific recognition of target messenger RNA (mRNA).[10] Drosha and Dicer cleavage is determined by certain RNA structures like a terminal loop region, a central stem bulge and single-stranded RNA flanking sequences, which are recognized and serve as reference points for endonuclease digestions.[5,6,11–13] In the case of miRNA processing by Drosha, the stem-single-stranded RNA junction is recognized by the Drosha cofactor DGCRG8 and cleavage occurs ~11 nt away from this structure.[13] Dicer anchors to both 5′ and 3′ ends of processed molecules and cleaves ~21–28 nt measured from one of the termini of the pre-miRNA or shRNA.[11] For Dicer cleavage mainly, the 5′ counting rules apply, meaning that the 5′ end acts as the primary reference point for the cleavage. The terminal loop is important as its disruption inhibits Drosha pri-miRNA processing as well as pre-miRNA and shRNA processing by Dicer.[13] Precise cleavage

Correspondence: *Pavlina Konstantinova, Meibergdreef 61, 1105 BA Amsterdam, The Netherlands. E-mail: p.konstantinova@uniQure.com*

is critical for shRNA and miRNA functions because alterations in cleavage sites can change the abundance and thermodynamic stability of the shRNA and miRNA duplex, which is important for RNA-induced silencing complex loading.[14]

shRNAs are generally expressed from polymerase III (pol III) promoters, which provide constitutive high expression levels necessary for potent knockdown of target mRNA. Although these features are valuable for research purposes, they can be disadvantageous for therapeutic applications. It has been reported that pol III-expressed shRNA can lead to severe toxicity when high doses are used.[15–17] Grimm *et al.*[17] observed liver failure and mortality in mice injected with different adeno-associated virus (AAV)-expressed shRNAs irrespective of hairpin length, sequence and target. Toxic side-effects were associated with saturation of the cellular RNAi machinery and changes in endogenous miRNA expression. Toxicity may be circumvented by using lower doses of vectors encoding shRNA. However, this approach may result in loss of RNAi silencing efficacy and therapeutic effect.[18] Alternatively, toxicity resulting from shRNA overexpression can be resolved by embedding the siRNA sequence into an artificial miRNA scaffold and expressing it from weaker polymerase II (pol II) promoters.[19,20] Incorporation of a siRNA sequence in an artificial miRNA scaffold has been shown to abolish shRNA-induced neuronal cell death and to avoid disruption of the endogenous RNAi pathway.[18,21] However, in some cases miRNAs were found to be less potent as compared with shRNAs.[22]

Another disadvantage of pol III-expressed shRNAs is their constitutive expression in all cell types and organs. In order to limit their expression to target organs, the use of tissue-specific promoters has been applied for shRNAs.[23,24] However, this has been achieved with limited success as the rules for efficient transcription of shRNAs from poll II promoters are poorly understood and these constructs show only mild knockdown efficacy. Others have used inducible systems regulated by tetracycline or by ecdysone for expression of shRNAs or artificial miRNAs, which allows time- and dose-dependent expression when the inducer is administered and no expression in its absence.[25–29] Proof of concept has been established in transgenic mice enabling inducible and reversible suppression of gene expression by a tetracycline-regulated shRNA which also resulted in phenotypic changes.[27] However, the use of such systems in preclinical and clinical studies is limited because they include two additional components; elements encoding regulatory proteins that often induce an immune response and inducer molecules which need to be safe for long-term applications.

To date, no detailed analyses have been performed on the processing of identical predicted siRNA sequences embedded in shRNA or artificial miRNA scaffolds and the consequences for *in vivo* applications. Moreover, long-term efficacy *in vivo* and the use of miRNA expressed from a tissue-specific promoter have not been described. We addressed these issues by incorporating identical predicted siRNA targeting apolipoprotein B (ApoB) in a shRNA (shApoB) or artificial miRNA scaffold (miApoB) and performed next generation sequencing (NGS) analysis of the processed small RNAs. In addition, aspecific off-target effects of shApoB and miApoB *in vivo* were investigated using NGS transcriptome analysis of the murine livers. ApoB is a constituent of all classes of lipoproteins that are considered atherogenic, and elevated ApoB levels have been demonstrated to correlate with increased risk of cardiovascular disease.[30] Therefore, ApoB is a highly validated target for treatment of increased low-density lipoprotein cholesterol levels and subsequent cardiovascular disease.[31,32] Injection of AAV-shApoB and AAV-miApoB yielded a long-term strong reduction of total cholesterol and ApoB expression. However, AAV-miApoB expressed from the liver-specific LP1 promoter induced stronger knockdown and its expression was restricted to the targeted hepatocytes in contrast to AAV-shApoB, which was ubiquitously expressed. Our results demonstrate that incorporation of identical predicted siRNA sequences in a shRNA or miRNA scaffolds yields differential processing and long-term efficacy *in vivo* that might have implications for future therapeutic applications.

RESULTS

In vitro efficacy of shApoB and miApoB

Previously, we have reported that AAV delivery of shApoB expressed from the H1 pol III promoter is highly effective in knocking down ApoB and in reducing plasma cholesterol in mice.[33] However, the AAV-shApoB effect measured at 8 weeks p.i. decreased as compared with week 2 p.i., which was associated with lower expression of anti-ApoB siRNA (siApoB).[33] For clinical applications, stringent control of shRNA expression and restriction to the target organs is desirable. Therefore, the 21 nt-long siApoB guide sequence was embedded in an artificial miRNA scaffold using pri-mir-155 (miApoB; **Figure 1a**) and expressed from the liver-specific LP1 promoter. The mature miApoB sequence was predicted to be identical as the one expressed from the shApoB scaffold (**Figure 1a**).

Initially, the efficacy of miApoB was tested *in vitro* using the cytomegalo virus promoter instead of the liver-specific LP1 promoter since the latter has low activity *in vitro*[34] The inhibitory effect of shApoB and miApoB was compared by co-transfecting human embryonic kidney 293T (HEK 293T) cells with a reporter expressing renilla luciferase that contained the ApoB target sequence in its 3′-untranslated region (Luc-ApoB). Scrambled controls for both shRNA and miRNA (shScr and miScr) were included as negative controls and firefly luciferase expression was measured to correct for transfection efficiency. The renilla/firefly luciferase ratio in the negative controls was set at 100% and relative inhibition of the Luc-ApoB reporter was calculated. Both shApoB and miApoB showed similar efficacy and reduced luciferase expression by ~80% (**Figure 1b**).

Since the identical predicted siApoB sequence was embedded in the shApoB or miApoB scaffold the number of processed molecules per cell was determined by small RNA Taqman assay (**Figure 1c**). HEK 293T cells were transfected with either shApoB- or miApoB-expression constructs and 2 days post-transfection total RNA was isolated and siApoB copies were measured. Processing of siApoB from the miApoB scaffold was ~30-fold lower as compared with shApoB (**Figure 1c**). In order to assess the effect of the inhibitory constructs on endogenous ApoB expression, the mouse hepatoma Hepa1–6 cell line was transfected with shApoB or miApoB and ApoB mRNA knockdown was measured 2 days post transfection (**Figure 1d**). Both shApoB and miApoB efficiently inhibited ApoB mRNA up to 80% confirming the efficacy and specificity of the hairpin constructs. Our results indicate that shApoB and miApoB are equally effective in inhibiting Luc-ApoB and endogenous ApoB mRNA expression *in vitro*.

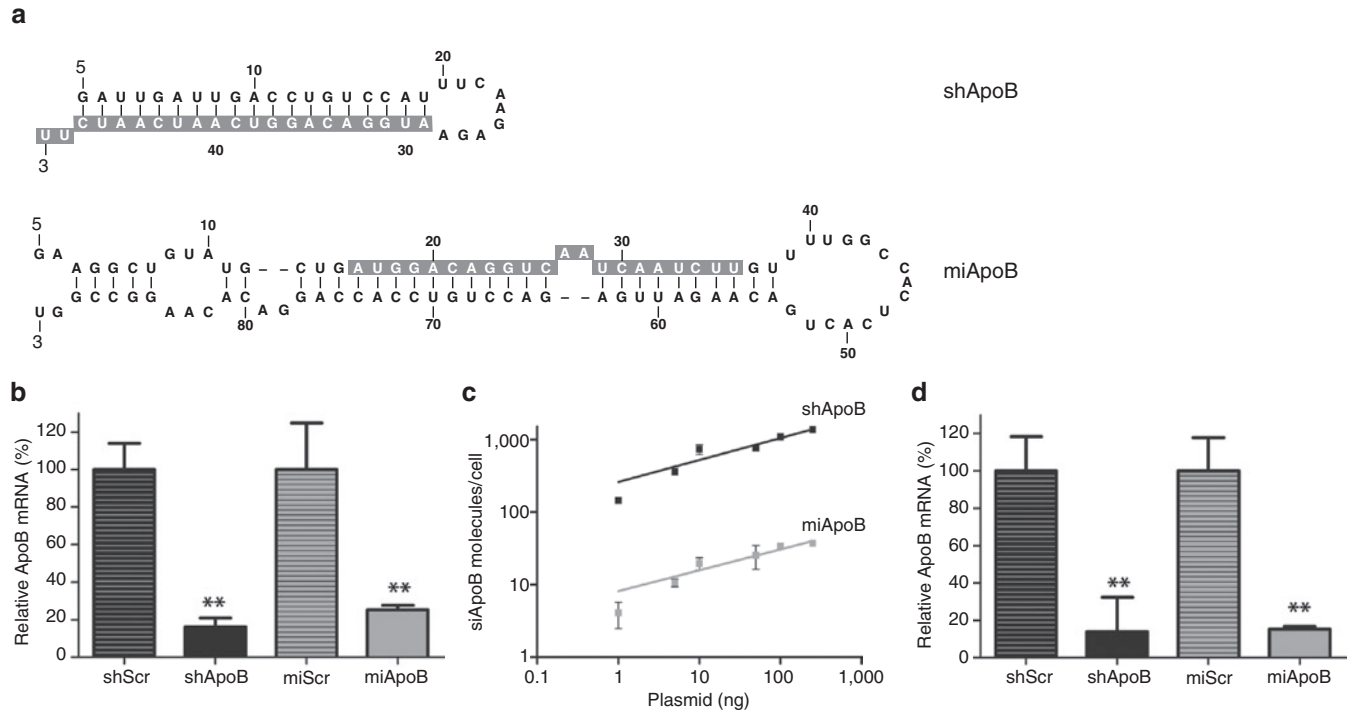

Figure 1 Structure and knockdown efficacy of apolipoprotein B100 (ApoB) in a shRNA (shApoB) and ApoB artificial miRNA scaffold (miApoB) *in vitro*. (**a**) Predicted stem-loop structure for shApoB and miApoB with the guide strand shown in gray. (**b**) Knockdown of Luc-ApoB by shApoB and miApoB in Hek293T cells. Renilla and firefly luciferase were measured 2 days post-transfection with 50 ng Luc-ApoB reporter and 50 ng shApoB or miApoB, and renilla luciferase expression was normalized to firefly luciferase expression. Scrambled controls for both shRNA and miRNA (shScr and miScr) served as negative controls and were set at 100%. Data are represented as mean values ± SD from three independent experiments analyzed with factor correction[52] $^{**}P < 0.01$ versus shScr or miScr. (**c**) Sequences targeting apolipoprotein B100 (siApoB) expression from shApoB and miApoB in Hek293T cells. RNA was isolated two days post-transfection with 1, 5, 10, 50, 100, and 250 ng of shApoB or miApoB and siApoB-specific small RNA TaqMan was performed. siApoB copy number was calculated using a siApoB synthetic RNA oligo standard line. Data are represented as mean values from two independent experiments conducted with two technical replicates. (**d**) Endogenous ApoB mRNA knockdown by shApoB and miApoB in Hepa1–6 cells. qRT-PCR was performed two days post-transfection with 1 µg shApoB or miApoB and ApoB mRNA levels were calculated relative to actin mRNA. shScr and miScr served as negative controls and were set at 100%. Data are represented as mean values + SD from a representative experiment conducted with three technical replicates. $^{**}P < 0.01$ versus shScr or miScr.

NGS analysis of siApoB processed from shApoB or miApoB scaffolds reveals guide and passenger strand heterogeneity

So far, the "golden standard" for siRNA detection has been the small RNA TaqMan assay that relies on amplification of the predicted processed guide strand, which is normally 21 nt long. In the current research we investigated whether exactly identical siRNA sequences are processed by the cellular RNAi machinery from shRNA and miRNA scaffolds. This is an important issue since it may have serious implications for future therapeutic development. NGS sequencing was performed on small RNAs isolated from HEK 293T cells transfected with shApoB or miApoB. A total of ~16 mln reads were obtained for each sample, which were further processed by applying the selection criteria described in Materials and Methods. For the NGS data analysis, all reads smaller than 15 nt or larger than 55 nt and all reads that were read <10 times were excluded from the analysis. Cellular miRNA expression pattern were compared between the miApoB and shApoB samples and are shown in **Supplementary Table S2** online. The small RNAs were aligned against their reference sequence resulting in 541.939 reads matching shApoB and 1.525.211 reads matching miApoB (**Supplementary Figures S1 and S2** online). Analysis of the length distribution of the reads indicated that siApoB guide strand originating from shApoB ranged between 19 and 23 nt, with the most abundant one being 21 nt-long (**Figure 2a**). Surprisingly, siApoB guide from miApoB scaffold ranged from 23 to 25 nt with the 24 nt-long strand being the predominant variant. This finding was rather unexpected considering that the predicted guide strand of siApoB was 21 nt long for both shApoB and miApoB scaffolds. Analysis of the processed 5′ ends of the siApoB guide strand indicated that most of the reads matched position +1 relative to the predicted cleavage site for shApoB, whereas all the reads matched position 0 for miApoB (**Figure 2b**). The 3′ ends of the siApoB guide strand had a more heterogeneous pattern and ranged from −1 to +3 for shApoB and +1 to +4 for miApoB (**Figure 2c**).

Next, we looked at the sequence distribution and percentage of reads for both the guide and passenger siApoB strands originating from the shApoB and miApoB scaffolds (**Figure 2d**). A substantial difference between the two is that the guide from shApoB is in the 3′ arm and hence Dicer[6] or other endonuclease[7–9] defines the cleavage position while the guide is present in the 5′ arm of miApoB, where Drosha defines the cleavage.[5] Therefore, defining the length and exact cleavage position for the guide and passenger strands is very important since even single nucleotide differences

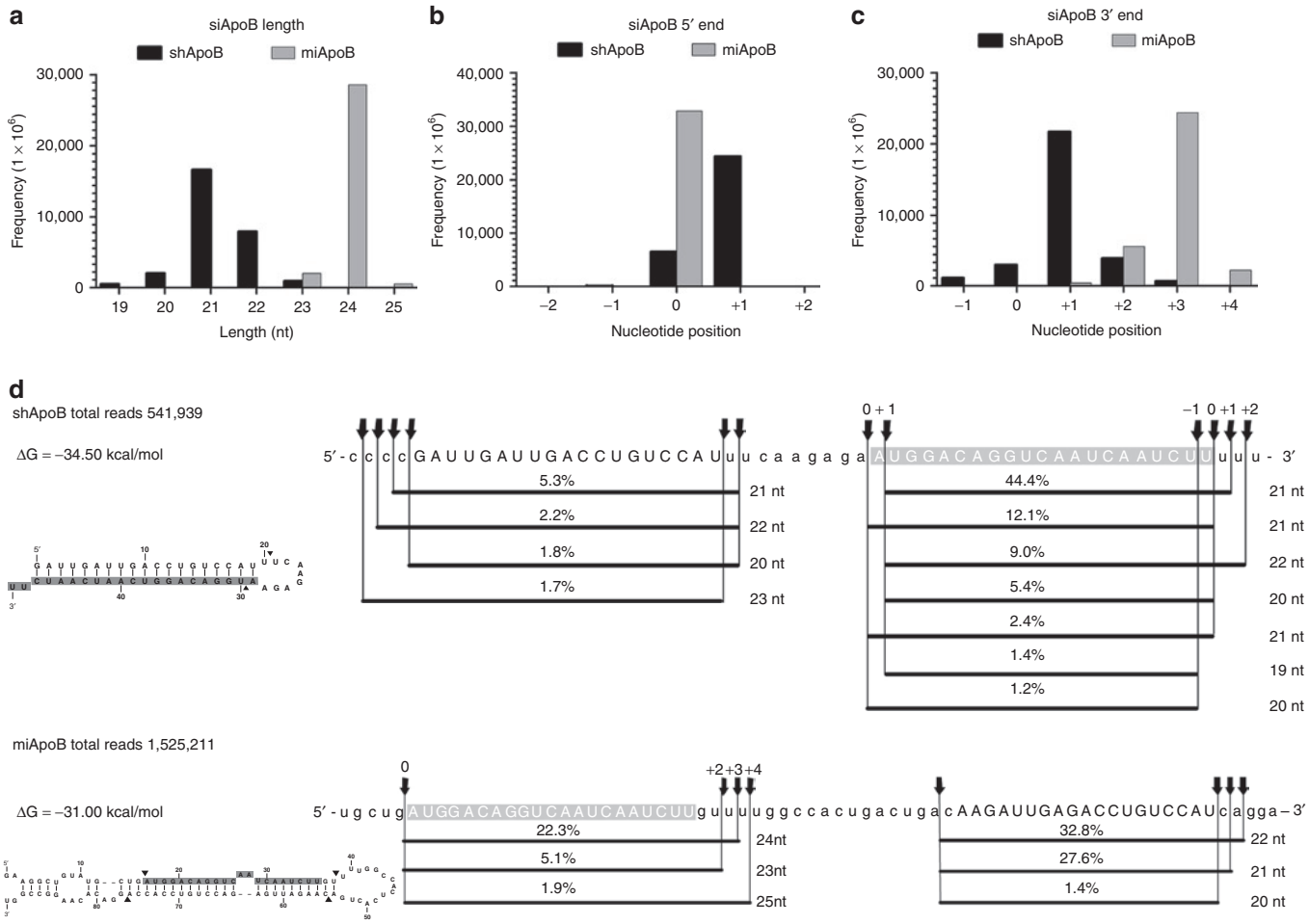

Figure 2 Small RNA next generation sequencing (NGS) analysis reveals differential sequences targeting apolipoprotein B100 (siApoB) guide and siApoB* passenger strand processing from apolipoprotein B100 (ApoB) in a shRNA (shApoB) and ApoB artificial miRNA scaffold (miApoB) scaffolds. (**a**) Sequence length distribution of the siApoB guide strand recovered from small RNA NGS of Hek293T cells transfected with shApoB- or miApoB-expression plasmids. The frequency on the *y* axis represents the reads per million. (**b**) Sequence variation in the 5′ end of the mature siApoB guide strand. Nucleotide position 0 was designated as the 5′ end of the predicted siApoB guide and other forms are numbered accordingly. (**c**) Sequence variation in the 3′ end of the mature siApoB guide strand. Nucleotide position 0 was designated as the 3′ end of the predicted siApoB guide and other forms are numbered accordingly. (**d**) Sequence distribution and percentage of reads from siApoB guide and siApoB* passenger strands aligned to the reference shApoB (upper panel) or miApoB (lower panel) sequence. ApoB sequences are presented in upper case, the loop and flanking sequences are in lower case, the predicted 21 nt siApoB guide strand is shaded in gray. The percentage of reads was calculated based on the total number of reads matching the reference shApoB or miApoB sequence. Sequences represented with less than 1% were excluded from the figure and can be found in **Supplementary Figures S1** and **S2** online.

may result in significant changes in the predicted targets of the siRNAs. Moreover, the passenger siRNA* strand, if not degraded efficiently, may bind to unanticipated targets and cause off-target effects. As expected, 44.4% of the reads originating from shApoB matched the siApoB guide strand but processing was shifted at position +1 (**Figure 2d**, upper panel). Surprisingly only 12.1% of the reads matched perfectly the predicted siApoB guide strand of 21 nt and starting at position 0. The reads matching the passenger siApoB* strand were represented in much lower percentage with the predominant one being only 5.3%.

Analysis of the guide strand from the siApoB reads originating from the miApoB scaffold indicated that they all started at the predicted cleavage site (**Figure 2d**, lower panel). Surprisingly, the predominant, 22.3% of reads were 24 nt-long. Furthermore 5.1% reads were 23 nt- and 1.9% were 25 nt-long. A substantial number of 62% of the reads was found matching the passenger siApoB* strand and ranged between 20 and 22 nt in length. In conclusion, both shApoB and miApoB scaffolds did not yield the predicted siApoB guide or siApoB* passenger sequences after processing from the cellular RNAi machinery. The guide from miApoB was cleaved much more precisely by Drosha at its 5′ end as compared with shApoB that gave more heterogeneous pools of sequences following processing. Cellular miRNA expression profiles were also not identical for cells transfected with shApoB or miApoB (**Supplementary Table S2** online).

Long-term knockdown efficacy of AAV-delivered shApoB and miApoB in murine liver

Having shown that cytomegalo virus-expressed miApoB, although differentially processed, is as effective in inhibiting ApoB as shApoB

in vitro, we replaced the constitutive cytomegalo virus promoter with the liver-specific LP1 promoter for *in vivo* applications. The use of LP1 limits miApoB expression to hepatocytes, thereby avoiding siApoB accumulation in nontarget tissues. Male C57Bl/6 mice were injected with 1×10^{11} gc self-complementary AAV8 (scAAV8) per animal encoding shApoB, miApoB, shScr, or miScr. All viruses co-expressed enhanced green fluorescent protein (eGFP) for monitoring of liver transduction efficacy. At week 27 p.i. mice were sacrificed and siApoB small RNA Taqman was performed on RNA isolated from the liver, spleen, ileum, lung, heart, and kidney. Four times less siApoB molecules were detected from the AAV-miApoB-injected animals in the liver as compared with AAV-shApoB-injected animals (1163 versus 399 copies per cell respectively) (**Figure 3a**). In addition, in AAV-miApoB-injected animals siApoB expression was restricted to the liver in contrast to AAV-shApoB-injected mice where expression was detected in nontarget organs (**Figure 3a**).

At week 27 p.i. ApoB mRNA was reduced by 55% in AAV-miApoB-injected animals whereas no mRNA decrease was detected in the AAV-shApoB group (**Figure 3b**). The inhibitory effect of AAV-shApoB and AAV-miApoB on ApoB protein was determined every 2 weeks up to week 27 p.i. by western blot (**Figure 3c** and data not shown). Initially, a strong inhibition of ApoB protein was achieved by both AAV-shApoB and AAV-miApoB. However, the effect decreased at week 10 p.i. for AAV-shApoB and at week 20 p.i. for AAV-miApoB. At week 27 p.i. ApoB concentrations in plasma were decreased by 25% in animals injected with AAV-shApoB and by 60% in mice treated with AAV-miApoB (**Figure 3c**). Next, the phenotypic effect of ApoB knockdown was measured every 2 weeks by biochemical lipid profiling of cholesterol in murine plasma (**Figure 3d**). Similar to the ApoB protein knockdown, initially a strong ~70% cholesterol decrease was induced by both AAV-shApoB and AAV-miApoB. However, the effect decreased gradually and at week 27 p.i. total cholesterol levels were reduced in both groups by only 25% as compared with scrambled controls (**Figure 3d**). Two-way ANOVA analysis revealed that AAV-miApoB performed significantly better than AAV-shApoB in reducing plasma cholesterol over the course of the experiment ($P = 0.0018$). In addition, there was a clear trend of a slower loss of plasma ApoB and cholesterol inhibition in mice injected with AAV-miApoB as compared with AAV-shApoB indicating that miApoB had a better long-term efficacy than shApoB (**Figure 3c,d**).

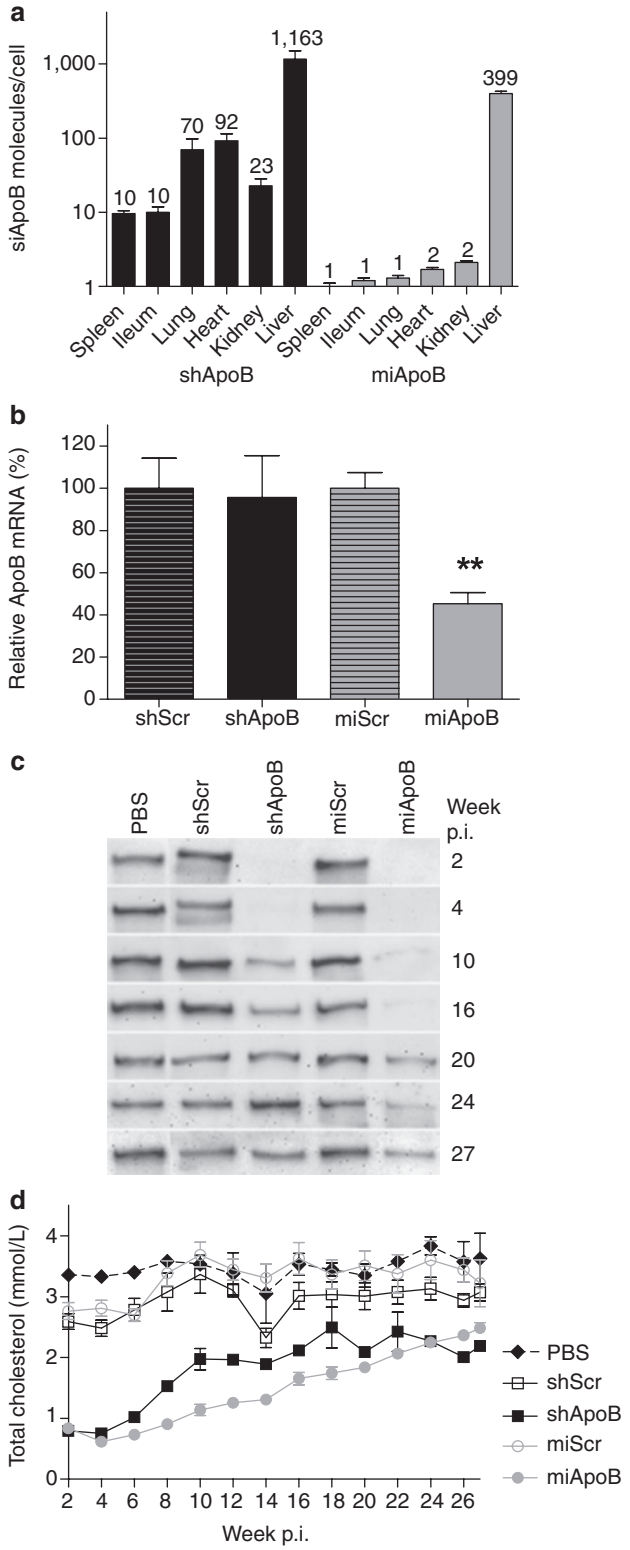

Figure 3 Long-term reduction of apolipoprotein B100 (ApoB) and plasma cholesterol levels by 1×10^{11} gc adeno-associated virus (AAV)-ApoB in a shRNA (shApoB) and AAV-ApoB artificial miRNA scaffold (miApoB). Mice were intravenously injected with 1×10^{11} gc AAV-shApoB or AAV-miApoB, or their respective controls AAV-scrambled control for shRNA (shScr), AAV-scrambled control for miRNA (miScr) or phosphate-buffered saline (PBS). Plasma was collected every two weeks p.i. and animals were sacrificed at 27 weeks p.i. (**a**) siApoB expression in murine spleen, ileum, lung, heart, kidney, and liver 27 weeks p.i. Total RNA was isolated from snap-frozen tissue and siApoB-specific small RNA TaqMan was performed. siApoB copy number was calculated using a siApoB synthetic RNA oligo standard line. Data are represented as mean values ± SE, treatment groups are $n = 4$–5 for AAV-shApoB, AAV-shScr, AAV-miApoB or AAV-miScr and $n = 2$ for PBS-injected animals. (**b**) Relative ApoB mRNA expression in murine liver 27 weeks p.i. Total RNA was isolated from snap-frozen liver tissue and qRT-PCR was performed using ApoB- and actin-specific primers. ApoB mRNA levels were calculated relative to actin mRNA and scrambled controls were set at 100 %. $^{**}P < 0.01$ versus shScr or miScr (**c**) Western blot analysis of plasma ApoB at 2, 4, 10, 16, 20, 24, and 27 weeks p.i. ApoB protein was detected in 0.1 µl plasma using a polyclonal antibody against ApoB. (**d**) Total cholesterol levels in plasma collected from fasted mice over the course of 27 weeks p.i. Cholesterol levels were analyzed on the automated clinical chemistry analyzer Modular Analytics P800.

Based on our previous observations that shApoB and miApoB are differentially processed and that miApoB has a different passenger, we checked for possible aspecific off-target effects *in vivo*. NGS liver transcriptome analysis was performed 8 weeks p.i. for animals injected with 1×10^{11} gc AAV encoding shScr, shApoB, miScr, and miApoB. We investigated whether shApoB and miApoB processing differences translate into differences in gene expression in injected animals. A total number of 266 genes were significantly changing ($P < 0.05$) in miApoB-injected mice compared to miScr (**Supplementary Table S3** online). In addition, 106 genes were found to be significantly up or down-regulated ($P < 0.05$) in the shApoB mice as compared with shScr (**Supplementary Table S4** online). Off-target predictions using Smith–Waterman algorithm[35] for the most abundant guide and passenger strand variants were performed to investigate if any of the observed changes results from aspecific interactions. None of the changing genes had predicted targets for the guide or passenger strands of shApoB or miApoB (**Supplementary Tables S3 and S4** online).

Decrease of ApoB knockdown is due to gradual AAV vector DNA loss

To follow up on the loss of ApoB and cholesterol inhibitory effect *in vivo*, AAV vector DNA copies were determined in murine liver at 2, 8, and 27 weeks p.i. from mice injected with AAV-shApoB and AAV-shScr. In both animal groups a clear gradual decrease in AAV vector DNA was observed over time indicating that the effect was not dependent on the shRNA target sequence (**Figure 4a**). At week 8 and 27 p.i. the amount of AAV vector DNA copies in murine livers from AAV-miApoB and AAV-miScr were similar to AAV-shApoB and AAV-shScr indicating similar kinetics of vector loss irrespective of the promoter type (pol III or pol II), target sequence (Scr or ApoB), or of the shApoB or miApoB scaffolds (**Figure 4b**).

The loss of AAV vector DNA occurs presumably as a result of cell death due to liver toxicity. In line with this assumption, transient activation of liver transaminases aspartate aminotransferase and alanine aminotransferase were measured in all AAV-injected animals during the course of the experiment (**Supplementary Figure S3** online). To explore the mechanism behind the DNA loss in more detail liver morphology was examined by hematoxylin and eosin staining. In addition, immunohistochemistry was performed to detect markers for apoptosis, T-regulatory cells, cytotoxic T lymphocytes, macrophages, and B lymphocytes. With none of those markers obvious differences between the treatment and phosphate-buffered saline groups were found (data not shown). ELISA assay for antibodies against eGFP was performed to explore the possibility that these could have contributed to the loss of AAV vector DNA. No immune response against eGFP was found in any of the animals (data not shown). Together, these results indicate that there was no acute inflammatory effect responsible for the loss of AAV vector DNA.

A possible reason for the observed AAV vector DNA loss is oversaturation of the endogenous RNAi machinery resulting in changes of cellular miRNA processing. Previously, we have shown that cellular mir-122, mir-29a and let-7a expression does not change in murine livers at 2 and 8 weeks p.i. with 1×10^{11} gc AAV-shApoB or AAV-shScr.[33] To exclude the possibility that the loss

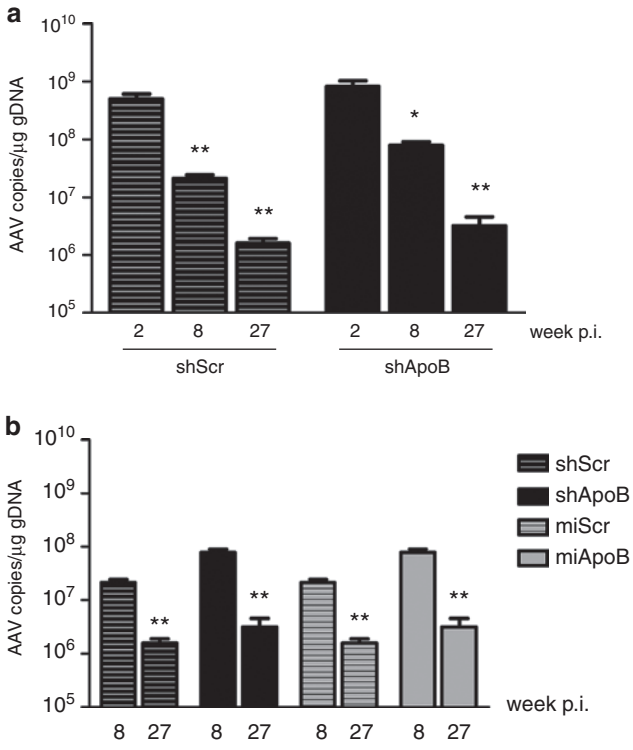

Figure 4 Gradual loss of AAV vector DNA *in vivo* over a time course of 27 weeks p.i. Mice were intravenously injected with 1×10^{11} gc adeno-associated virus (AAV)-apolipoprotein B (ApoB) in a shRNA (shApoB) or AAV-ApoB artificial miRNA scaffold (miApoB), or their respective controls AAV-scrambled control for shRNA (shScr) and AAV-scrambled control for miRNA (miScr) and livers were collected at 2, 8, or 27 weeks p.i. Genomic DNA (gDNA) was isolated from snap-frozen liver tissue and qPCR was performed using LP1-specific primers. AAV copy number was calculated using a LP1 plasmid standard line. (**a**) AAV copy number per microgram gDNA in murine liver of animals injected with AAV-shScr or AAV-shApoB at 2, 8, and 27 weeks p.i. *$P < 0.05$, **$P < 0.01$ versus shScr wk2 or shApoB wk2. (**b**) AAV copy number per microgram gDNA in murine liver 8 and 27 weeks p.i. with AAV-shScr, AAV-shApoB, AAV-miScr, or AAV-miApoB. Data are represented as mean values ± SE, treatment groups are $n = 4–5$.

of AAV vector DNA is due to oversaturation of the endogenous miRNA pathway, we determined the amount of the most abundant liver miRNA mir-122 at week 27 p.i. for animals injected with AAV-shApoB, AAV-miApoB, and the two control viruses. There were no significant changes in mir-122 expression between all animal groups indicating that there was no oversaturation of the RNAi machinery caused by the injected AAVs (**Supplementary Figure S4** online).

Lower AAV dose results in sustained ApoB and plasma cholesterol decrease

A possible reason for the observed AAV vector DNA loss and decrease in ApoB knockdown effect is the use of a too high viral dose. Previously we have shown that when 1×10^{9} gc AAV-shApoB or AAV-shScr was injected in mice, ~90% liver transduction can be achieved that was not associated with viral loss at 8 weeks p.i.[33] In this study, a 12-week mouse experiment was initiated with a dose of 5×10^{9} gc AAV-shApoB, AAV-miApoB, AAV-shScr, AAV-miScr, and an additional control group AAV-eGFP expressing only eGFP

(Figure 5). The experiment was restricted to 12 weeks based on our previous observations[33] and the results presented in Figure 3 showing that a 12-week time period is sufficient to observe a significant loss of AAV vector DNA and knockdown efficacy.

Inhibition of ApoB mRNA was observed in the groups injected with AAV-shApoB or AAV-miApoB at 12 weeks p.i, 57% for AAV-miApoB and 43% for AAV-shApoB, respectively (Figure 5a). Subsequently a decrease in ApoB protein levels was observed at week 4 and the effect remained stable during the 12-week course of the experiment (Figure 5b). Plasma cholesterol levels were determined every 2 weeks to study the kinetics and longevity of ApoB knockdown (Figure 5c). Two weeks p.i., plasma cholesterol levels were decreased by 53% and 39% for AAV-miApoB- and AAV-shApoB-injected animals and the effect remained stable until week 12 p.i. Finally, equal amounts of AAV vector DNA copies were measured in mice livers for all animal groups (Figure 5d). The animals injected with AAV-eGFP control had similar ApoB, and cholesterol levels as well as AAV vector DNA copies as the AAV-shScr or AAV-miScr controls indicating that there were no hairpin-related nonspecific toxic effects in the current study. Importantly, over the 12-week time course, liver transaminases were not significantly elevated for all treatment groups (**Supplementary Figure S5** online). Again, there was a trend for a stronger ApoB and cholesterol decrease in AAV-miApoB injected animals as compared with AAV-shApoB (Figure 5b,c).

DISCUSSION

RNAi technology is one of the fastest developing scientific fields and holds a great promise for development of therapeutics of various diseases in the liver, brain, and the eye.[36] AAV vectors mediating expression of shRNAs or artificial miRNAs have proven to be valuable vehicles for RNAi research and therapy. However, induction of severe toxicity and/or off-target effects remains a major hurdle to be overcome before a long-term inhibition of a disease-related gene in the target tissue or organ can be accomplished. So far, detailed studies analyzing the precise processing of siRNA molecules expressed from shRNA or miRNA scaffolds and the consequences for *in vivo* applications have not been carried out. To address this issue, we have performed detailed NGS analysis of the siRNA processing when identical predicted sequences targeting ApoB have been embedded in shRNA or miRNA scaffolds. By using AAV delivery, we compared the efficacy and toxicity profiles of a constitutively expressed shRNA to tissue-specific expressed artificial miRNA in long-term *in vivo* studies.

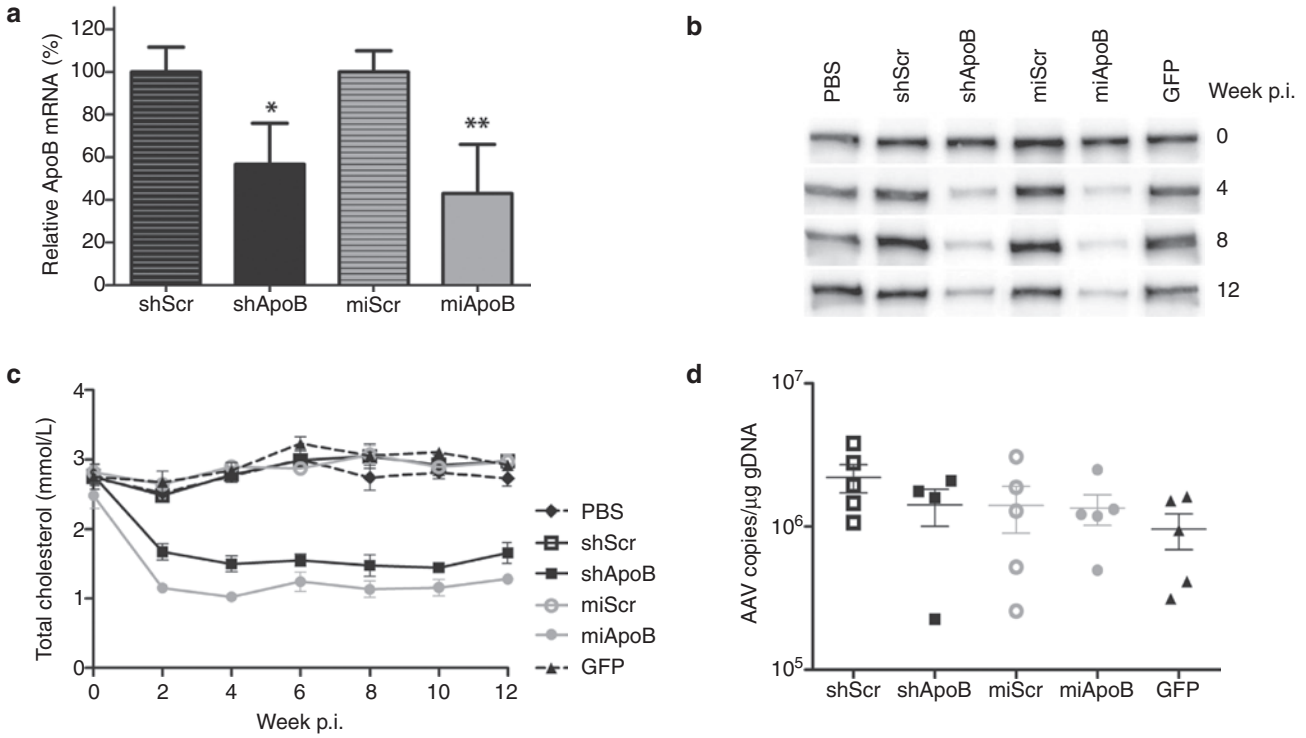

Figure 5 Sustained decrease of apolipoprotein B100 (ApoB) and plasma cholesterol levels by 5 × 10^9 gc adeno-associated virus (AAV)-ApoB in a shRNA (shApoB) and AAV-ApoB artificial miRNA scaffold (miApoB). Mice were intravenously injected with 5 × 10^9 gc AAV-shApoB, AAV-miApoB, AAV-scrambled control for shRNA (shScr), AAV-scrambled control for miRNA (miScr), AAV-green fluorescent protein (GFP), or phosphate-buffered saline (PBS). Plasma was collected every 2 weeks p.i. and animals were sacrificed at 12 weeks p.i. (**a**) Relative ApoB mRNA expression in murine liver 12 weeks p.i. Total RNA was isolated from snap-frozen liver tissue and qRT-PCR was performed using ApoB- and actin-specific primers. ApoB mRNA levels were calculated relative to actin mRNA and scrambled controls were set at 100%.*$P < 0.05$, **$P < 0.01$ versus shScr or miScr (**b**) Western blot analysis of plasma ApoB at 0, 4, 8, and 12 weeks p.i. ApoB protein was detected in 0.1 µl plasma using a polyclonal antibody against ApoB. (**c**) Total cholesterol levels in plasma collected from fasted mice over the course of 12 weeks p.i. Cholesterol levels were analyzed on the automated clinical chemistry analyzer Modular Analytics P800. (**d**) AAV copy number per microgram gDNA in murine liver 12 weeks p.i. gDNA was isolated from snap-frozen liver tissue and qPCR was performed using GFP-specific primers. AAV copy number was calculated using a GFP plasmid standard line. Data are represented as mean values ± SE, treatment groups are $n = 4–5$.

An unexpected discovery in the current study was that siRNA processing by the cellular RNAi machinery did not follow the generally accepted and described cleavage sites for both molecules shApoB and miApoB siApoB guide strand originating from the shApoB scaffold was more heterogeneous in cleavage sites and length as compared with the product originating from the miApoB scaffold. Most likely, differential cleavage mechanism defined the heterogeneity in the guide and passenger strands. In addition, shRNAs with 19 bp stem or less are not necessarily recognized by Dicer and maybe be processed differently.[7–9] The heterogeneity seen with the shApoB can also be explained by the potential for two or three uridines to be added following termination of pol III transcription.[37] The main pool of guide sequences originating from miApoB was 24 nt-long although we used the scaffold of cellular pri-mir-155 that produces a 23 nt mature miRNA. However, a 24 nt-long siApoB sequence did not compromise efficacy because when placed in the miApoB scaffold, the ApoB target sequence was extended at the 3′ end with 4 nt until the loop (**Figure 1a**).

Another important observation is that the siApoB* passenger strand was present in a very high percentage of the reads from miApoB. Our results are in accordance with Gu *et al.*[14] who recently reported that mainly the guide siRNA strand of an shRNA was pulled down with Ago2 while both guide and passenger strands were detected from a miRNA scaffold associated with Ago1/2/3/4. Moreover, the passenger strand from the miRNA scaffold was not cleaved and eliminated as efficiently as from the shRNA. However, reporter assays revealed that the passenger siRNA* strand was mainly loaded into nonactivated Ago complexes rendering those sequences ineffective at inducing knockdown. Our findings, together with the previously reported ones indicate that differential Ago loading of siRNAs originating from different scaffolds may have serious implications for future design of RNAi-based therapeutics.

There are important consequences of our findings for the small RNA Taqman that is being used for routine detection of siRNA expression. In our opinion this assay cannot be directly applied for sequences originating from shRNA or miRNA scaffolds because it amplifies only the predicted 21 nt guide strand and conclusions based on such data should be drawn with caution. Considering the different siApoB processing pattern from shApoB or miApoB scaffolds, the Small RNA Taqman that was performed *in vivo* has only an indicative value rather than a precise estimation of the number of molecules per cell.

The use of the liver-specific LP1 promoter for miApoB limited the expression of siApoB to hepatocytes, thus providing an additional safety level for future clinical applications compared to the ubiquitously expressed shApoB. So far it has been suggested that the use of tissue-specific promoters for miRNA expression will not be feasible *in vivo* as the expression would be too low to achieve significant therapeutic effect.[36] In the current study we provide evidence for the efficacy of such an approach *in vivo* and demonstrate its advantages over the pol III-expressed shRNA. Although it has been reported that expression of shRNA can be achieved from liver-specific hAAT promoter and tetracycline-inducible promoter,[23,27] the rules for design of potent shRNA expressed from pol II promoters are still far from clear. An additional advantage is that several miRNAs can be expressed as clusters from longer transcripts, allowing simultaneous targeting of multiple genes.[20,38,39] This feature of the miRNA is very important when mutation-prone viruses, such as HIV-1 or HCV, are targeted or when several disease-related genes need to be simultaneously silenced. Moreover, miRNAs can be linked to the 3′ untranslated region of a therapeutic gene, which is an additional advantage for therapeutic applications since it allows co-delivery of a codon-optimized gene together with a miRNA targeting the disease-causing version of the same gene. Such combinational therapy has been shown for alpha1-antitrypsin (AAT) deficiency, in which a hairpin RNA targeting mutated AAT transcript was delivered together with codon-optimized AAT gene.[40,41]

In this study, we have demonstrated a more sustained ApoB target knockdown by miApoB over the shApoB in long-term *in vivo* experiments. Although differential processing resulting in different siApoB families from the two scaffolds should be kept in mind, this study provides indication that limiting siRNA expression to the target cells or organ holds greater promises for future therapeutic applications. Oversaturation of the RNAi machinery and competition with cellular miRNA transport from nucleus to cytoplasm have been described for both siRNA and shRNA and this toxicity problem was circumvented when the siRNA sequence was expressed from a miRNA scaffold by the cytomegalo virus pol II promoter.[20,42] Grimm *et al.*[17] reported that delivery of a high dose of 1×10^{12} gc per animal scAAV8 expressing shRNA led to hepatocyte death, often severe enough to cause liver failure and morbidity. This was associated with accumulation of shRNA precursor, which saturated Exportin 5 and led to deregulation of the endogenous RNAi pathway. Toxic effects were reduced without compromising knockdown efficacy of the shRNA when a tenfold lower viral dose or liver-specific expression of the shRNA were used.[23] Several other studies revealed neurotoxicity following AAV delivery of a shRNA targeting Huntingtin mRNA.[18,21,22] Subsequently, when siRNA sequences were incorporated in an artificial miRNA scaffold and expressed from the U6 pol III promoter neurotoxicity was abolished.[21] To our knowledge, no long-term head-to-head comparison has been performed to evaluate the processing and efficacy of siRNA sequences incorporated as identical predicted guide strand in a pol III-shRNA or liver-specific LP1 pol II-miRNA scaffolds. In contrast to the above-mentioned studies, our current data demonstrate that LP1-expressed miApoB did not circumvent liver toxicity and vector DNA loss when high doses of AAV were injected into mice. In our case AAV-shApoB and AAV-miApoB delivery initially showed strong inhibition of ApoB protein and plasma cholesterol levels *in vivo* and the effects diminished due to gradual AAV vector DNA loss. Of note, the NGS small RNA analysis indicated that the number of processed siApoB molecules from the shApoB or miApoB scaffolds was almost identical indicating that we might have reached a threshold above which no more siRNA molecules are being processed. Indeed, it has been calculated that in a typical mammalian cell the number of active RNA-induced silencing complex complexes ranges from 10^3 to 10^4 and the number of ectopic RNAi triggers should be kept in this range.[43] An important observation was that none of the changes in gene expression in AAV-miApoB and AAV-shApoB can be explained by possible aspecific down-regulation of nontarget transcripts. Because of the complexity of sh/miRNA processing

and RNA-induced silencing complex loading, off-targeting interactions are difficult to predict and evaluate. Although we could not explain the changes in gene expression by off-target prediction with Smith–Waterman algorithm, we cannot exclude that other prediction methods like screening 3′-untranslated region of genes for perfect complementarity to siRNA seed region may be more accurate.[44] miRNAs may regulate their targets by translational repression, therefore we might speculate that the off-target effects may be stronger at protein level.

By lowering the viral dose 20-fold a stable reduction of ApoB protein and plasma cholesterol was achieved by both AAV-shApoB and AAV-miApoB. Ongoing research including detailed liver histology to determine liver damage and small RNA NGS from murine livers will further investigate the exact cause of loss of RNAi inhibitory effect. For example, it is still unclear why after 27 weeks substantial amounts of siApoB can be detected from the AAV-shApoB-injected animals without observing ApoB knockdown effect. GFP fluorescence microscopy analysis demonstrated that only a few positive cells were still present at 27 weeks p.i. Most likely, only those few cells still expressed siApoB, which was not enough to achieve overall ApoB inhibition effect since the majority of hepatocytes lost the siApoB due to liver regeneration. AAV itself is not likely to cause liver toxicity as it was shown not to be pathogenic or immunogenic in rodents[45] and in our studies we could not detect toxicity resulting from GFP expression, therefore excluding those two possibilities as reasons for AAV viral DNA loss.

In summary, our results demonstrate that incorporating identical predicted sequences in shRNA or miRNA scaffolds results in differential siRNA processing patterns that may have serious consequences for future RNAi-based therapeutic applications. However, we consider that tissue-specific expression and embedding siRNA in artificial miRNA scaffold can contribute to a better and safer gene therapy approach due to the intrinsic characteristics of the miRNA structure rendering it a better substrate for the RNAi machinery.

MATERIALS AND METHODS

DNA constructs. Cloning of shApoB constructs (shA10) and shScr in the pSuper and AAV backbone has been described previously.[33] To create the miApoB vector, the siRNA sequence from shApoB was cloned into the mir-155 backbone of pcDNA6.2-GW/EmGFP-miR (Invitrogen, Carlsbad, CA) by annealing complementary oligonucleotides and ligation into BamHI- and XhoI-digested pcDNA6.2 plasmid. As a negative control for miApoB pcDNA6.2-GW/EmGFP-miR-neg control (Invitrogen) was used, named miScr. The luciferase reporter Luc-ApoB containing in the 3′-untranslated region 1,851 nucleotides of the last exon from human ApoB has been described previously.[33] The sequences of the oligonucleotides used in this study are listed in **Supplementary Table S1** online.

Cell culture and transfections. The HEK293T and Hepa1–6 cell lines were maintained in Dulbecco's modified Eagle's medium (DMEM; Invitrogen) containing 10% fetal calf serum, 100 U/ml penicillin and 100 U/ml streptomycin, at 37 °C and 5% CO_2. For luciferase assays, endogenous ApoB knockdown assays, siRNA expression analysis, and small RNA NGS cells were seeded in 96-, 24-, or 6-well plates at a density of 3×10^4, 1.2×10^5, or 4.5×10^5 cells per well, respectively, in DMEM one day prior transfection. Transfections were performed with Lipofectamine 2000 reagent (Invitrogen) according to the manufacturer's instructions.

Luciferase assays. Cells were co-transfected with 50 ng Luc-ApoB that contains both firefly and renilla luciferase genes, and 50 ng shApoB or miApoB-expression constructs. Transfected cells were assayed at 48 hours post-transfection in 20 µl 1× passive lysis buffer (Promega, Madison, WI) by gentle rocking for 15 minutes at room temperature. The cell lysates were centrifuged for 5 minutes at 4000 rpm and 10 µl of the supernatant was used to measure firefly and renilla luciferase activities with the Dual-Luciferase Reporter Assay System (Promega). Relative luciferase activity was calculated as the ratio between renilla and firefly luciferase activities.

RNA isolation and quantitative real-time RT-PCR. To determine endogenous ApoB mRNA knockdown by shApoB and miApoB constructs *in vitro*, Hepa1–6 cells were transfected with 1 µg shApoB- or miApoB-expression plasmids using Lipofectamine 2000 reagent and total RNA was isolated from cells 48 hours post-transfection using the Nucleospin kit (Clontech, Mountain View, CA). For NGS analysis and small RNA Taqman Hek293T cells were transfected with 4 µg shApoB- or miApoB-expression plasmids using Lipofectamine 2000 reagent and total RNA was isolated from cells 48 hours post-transfection using Trizol (Invitrogen) according to the manufacturer's protocol. To determine ApoB mRNA knockdown *in vivo*, total RNA was isolated from frozen liver sections at 27 and 12 weeks p.i. using Trizol (Invitrogen). Genomic DNA was removed by DNase treatment using TURBO DNase (Ambion, Austin, TX). First strand cDNA was reverse transcribed using random hexamer primers with the Dynamo kit (Finnzymes, Espoo, Finland). Real time PCR amplification was performed with ApoB- and beta actin-specific primers (**Supplementary Table S1** online). PCR reaction conditions were: 95 °C for 10 minutes, followed by 40 cycles of 15 seconds at 95 °C and 1 minute at 60 °C. The assays were performed on ABI 7000 or ABI 7500 (Applied Biosystems, Foster City, CA). ApoB expression levels were normalized to beta actin as an internal control, and the relative gene expression $2^{-\Delta\Delta Ct}$ method of Livak and Schmittgen was used for analysis of PCR data.[46]

siRNA and miRNA detection by small RNA Taqman assay. RT reactions for siApoB and murine mir-122 expression were performed with the TaqMan MicroRNA Reverse Transcription Kit (Applied Biosystems) using 10 ng RNA and 3 µl custom-made specific RT-stem-loop primer (Applied Biosystems) according to the manufacturer's instructions. Amplification of the beta actin gene was used as a RNA quality and loading control.siRNA copy number per cell was calculated based on the amplification plot of a dilution series of synthetic siApoB RNA standard (IDT, Coralville, IA). The trend line value of the standard line was used to calculate the siApoB copy number cell, assuming 15 pg RNA per cell.[47]

NGS of small RNA. Small RNA sequencing libraries were generated using high-quality total RNA as input and the NEXTflex Small RNA Sequencing kit (Bioo Scientific, Austin, TX). Briefly, the small RNA species were subjected to ligation with 3′ and 5′ RNA adapters, first strand reverse transcription, and PCR amplification. Sample-specific barcodes were introduced in the PCR step. The PCR products were separated on TBE-PAGE electrophoresis and the expected band around 140–160 bp was recovered for each sample. The resulting sequencing libraries were quantified on a BioAnalyzer (Agilent, Santa Clara, CA). The libraries were multiplexed, clustered, and sequenced on an Illumina HiSeq 2000 (TruSeq v3 chemistry) with a single-read 36 cycles sequencing protocol and indexing. The sequencing run was analyzed with the Illumina CASAVA pipeline (v1.8.0), with demultiplexing based on sample-specific barcodes. The raw sequencing data produced was processed removing the sequence reads which were of too low quality (only "passing filter" reads were selected), and discarding reads that aligned against the PhiX control. In total, we generated 16016701 reads for sample miApoB, and 15843150 reads for sample shApoB.

The NGS small RNA raw data set was analyzed using the CLC_bio genomic workbench (CLC Bio, Aarhus, Denmark). The obtained reads were adaptor-trimmed, which decreased the average read size from ~36 bp to ~25 bp. The custom adapter sequenced used for trimming all the bases extending 5′ was: GTGACTGGAGTTCC- TTGGCACCCGAGAATTCCA. All reads containing ambiguity N symbols, reads shorter than 15 nt, longer

than 55 nt in length and reads represented <10 times were discarded. Next, both data sets from shApoB and miApoB samples were grouped based on the match to the reference sequence and the obtained unique small RNAs were aligned to the sequence of pre-miApoB: GATCCTGGAGGCTTGC-TGA AGGCTGTATGCTGATGGACAGGTCAATCAATCTTGTTTTGGCCA CTGACTGACAAGATTGAGACCTGTCCATCAGGACACAAGGCCTG TTACTAGCACTCACATGGAACAAATGGCCCAGATCTGGCCGCAG or shApoB: GATCCCCGA TTGATTGACCTGTCCATTTCAAGAGAA TGGACAGGTCAATCAATC-TTTTTCAGCTT sequence, respectively. To relatively represent the expression counts for the small RNAs obtained in the experiment, reads per million (rpm)[48] or percentage of reads based on the total number of reads matching the reference shApoB or miApoB sequence were calculated. Finally, to identify the differences in cellular miRNA reads between the miApoB and shApoB samples the small RNA data sets were annotated to miRBase, Release 18 and grouped based on the mature miRNA sequences, the rpm were calculated and the fold change between miApoB and shApoB samples was calculated.

Total RNA sequencing libraries for the Illumina sequencing platform were generated using high-quality total RNA as input and the Illumina TrueSeq RNA v2 Sample preparation kit according to the manufacturer's protocol. Each read file (sample), in the FASTQ format, was individually aligned against the mouse reference genome (15 May 2012 NCBI build 38.1) using CLC Bio-Genomic Workbench and the expression abundance for each gene (RPKM) was calculated according to Montazavi *et al.*[49] Smith–Waterman algorithm[35] was used to predict off-target genes in the mouse reference genome and mouse RNA Refseq for the most abundant expressed passenger and guide strands variants of shApoB and miApoB.

The NGS data discussed in this publication have been deposited in NCBI's Gene Expression Omnibus[50] and are accessible through GEO Series accession number GSE39187 (http://www.ncbi.nlm.nih.gov/geo/query/acc.cgi?acc=GSE39187).

Western blot analysis for detection of ApoB protein. Murine plasma proteins (0.1 µl) were separated by electrophoresis on a 3–8% Tris-Actetate gel (Invitrogen) and blotted onto a 0.45 µm nitrocellulose membrane (Invitrogen). The blot was incubated with a 1:2000 dilution of a rabbit polyclonal anti-ApoB antibody (ab31992, Abcam, Cambrigde, UK), followed by incubation with a 1:2000 dilution of goat anti-rabbit antibody conjugated to horseradish peroxidase (P0448, Dako, Glostrup, Denmark). Antibody binding was detected by the Lumi-LightPLUS chemiluminescent detection kit (Roche Diagnostics, Basel, Switzerland).

AAV vector production. Production of scAAV8 vectors encoding shApoB and shScr has been described previously.[33] The eGFP-expressing scAAV8 vector was created by digestion of a pTRCGW vector with XbaI and AflII restriction enzymes, blunting and ligation into a pro-AAV vector. The product of this cloning was named pVD287 and contains the eGFP gene under the control of the liver-specific LP1 promoter and generates scAAV due to a mutation in one terminal repeat For cloning the miRNA constructs, expression cassettes were amplified using PCR with specific primers miRf and miRr containing respectively EcoRI and PstI restriction sites at the 5′ end. Digested PCR product was ligated into EcoRI and PstI sites of pVD287. Constructs were sequence-verified and the presence of two inverted terminal repeats was confirmed by restriction digestion with SmaI. scAAV8 vectors were produced by calcium phosphate-mediated co-transfection in HEK293T cells, using the three-plasmid based system described by Gao *et al.*[51] Cells were lysed 48 hr after transfection and virus was released by addition of Tris lysis buffer. Crude lysate from all batches was treated with Benzonase (50 U/ml) (Merck, Darmstadt, Germany) for 1 hour at 37 °C. AAV vector particles were purified by iodixanol (Sigma, St Louis, MO) gradient centrifugation as described previously Purified batches were concentrated by passage through Vivaspin 15R tubes (Sartorius Stedim, Aubagne, France) and final concentration was determined by quantitative PCR with LP1f and LP1r primers amplifying a 95-bp fragment from the LP1 promoter region (**Supplementary Table S1** online). All viruses used in this study were simultaneously quantified three times to ensure that equal amount of gc per animal was injected.

Genomic DNA isolation and PCR. Genomic DNA was isolated using the DNeasy Blood & Tissue Kit (QIAGEN, Chatsworth, CA).according to the manufacturer's protocol The amount of viral DNA in 250 ng genomic DNA was quantified using quantitative PCR using Lp1fv and Lp1rv primers (**Supplementary Table S1** online) amplifying 95-bp fragment from LP1 region or primers eGFPf and eGFPr (**Supplementary Table S1** online) amplifying a 101-bp fragment from the eGFP region. As a standard line, serial dilutions of plasmid DNA containing LP1 or GFP respectively were used.

In vivo *experiments.* All animal experiments were conducted according to the guidelines of the local animal welfare committee. Six-to-eight-week-old male C57BL/6 mice received an intravenous AAV injection of 1×10^{11} gc per animal (~4×10^{12} gc/kg) or 5×10^{9} gc per animal (~2×10^{10} gc/kg) via the tail vein. Treatment groups were $n = 4$–5 for AAV-shRNA and AAV-miRNA and $n = 2$ for phosphate-buffered saline-injected animals. In the AAV-shApoB group sacrificed at 12 weeks $n = 4$ because one animal died during blood sampling. Heparinized blood samples were taken every two weeks p.i. from fasted mice. Mice were sacrificed at 2, 8, 12, or 27 weeks p.i. and liver, heart, lung, kidney, ileum, spleen, and plasma were collected for analysis. Liver samples from 2 and 8 weeks p.i. were obtained from a previous experiment where mice were injected with 1×10^{11} gc of identical preparation of AAV-shScr or AAV-shApoB. Mice were housed six per cage and feeding was performed *ad libitum* with regular chow. Plasma levels of alanine aminotransferase, transaminases aspartate aminotransferase, and total cholesterol were analyzed on the automated clinical chemistry analyzer Modular Analytics P800 (Roche Diagnostics) at the Academic Medical Center (Amsterdam, the Netherlands). Statistical analysis was performed by ANOVA testing and $P < 0.05$ was considered significant.

SUPPLEMENTARY MATERIAL

Figure S1. Sequence annotation of siApoB reads matching shApoB sequences.
Figure S2. Sequence annotation of siApoB reads matching miApoB sequences.
Figure S3. Transient increase in liver transaminases after injection with $1x10^{11}$ gc AAV.
Figure S4. No significant change in mir-122 expression after injection with AAV-shRNA and AAV-miRNA.
Figure S5. Stable liver transaminases after injection with $5x10^{9}$ gc AAV.
Table S1. Oligonucleotides used in this study.
Table S2. Changes in miRNA expression in shApoB versus miApoB samples.
Table S3. Expression changes in miApoB versus miScr murine liver samples.
Table S4. Expression changes in shApoB versus shScr murine liver samples.

ACKNOWLEDGMENTS

The authors thank Valerie Sier-Ferreira, Karin Kwikkers and Lizzy Comijn (uniQure biopharma b.v.) for their expertise on immunology aspects of this paper. We also thank Wim Hermens (uniQure) and Tita Ritsema (uniQure biopharma b.v.) for critically reviewing the manuscript. The self-complementary AAV vector containing the LP1 promoter was kindly provided by Amit C. Nathwani (St. Jude Children's Research Hospital, Memphis, TN) and the pTRCGW vector was kindly provided by Wim Hermens (uniQure biopharma b.v.) and Paul Dijkhuizen (The Netherlands Institute for Brain Research, Amsterdam, The Netherlands). The authors declare no conflict of interest.

REFERENCES

1. Pillai, RS (2005). MicroRNA function: multiple mechanisms for a tiny RNA? *RNA* **11**: 1753–1761.
2. Stark, A, Brennecke, J, Bushati, N, Russell, RB and Cohen, SM (2005). Animal MicroRNAs confer robustness to gene expression and have a significant impact on 3′UTR evolution. *Cell* **123**: 1133–1146.

3. Castanotto, D and Rossi, JJ (2009). The promises and pitfalls of RNA-interference-based therapeutics. *Nature* **457**: 426–433.
4. Mockenhaupt, S, Schürmann, N and Grimm, D (2011). When cellular networks run out of control: global dysregulation of the RNAi machinery in human pathology and therapy. *Prog Mol Biol Transl Sci* **102**: 165–242.
5. Zeng, Y, Yi, R and Cullen, BR (2005). Recognition and cleavage of primary microRNA precursors by the nuclear processing enzyme Drosha. *EMBO J* **24**: 138–148.
6. MacRae, IJ, Zhou, K and Doudna, JA (2007). Structural determinants of RNA recognition and cleavage by Dicer. *Nat Struct Mol Biol* **14**: 934–940.
7. Ge, Q, Ilves, H, Dallas, A, Kumar, P, Shorenstein, J, Kazakov, SA *et al.* (2010). Minimal-length short hairpin RNAs: the relationship of structure and RNAi activity. *RNA* **16**: 106–117.
8. Ge, Q, Dallas, A, Ilves, H, Shorenstein, J, Behlke, MA and Johnston, BH (2010). Effects of chemical modification on the potency, serum stability, and immunostimulatory properties of short shRNAs. *RNA* **16**: 118–130.
9. Siolas, D, Lerner, C, Burchard, J, Ge, W, Linsley, PS, Paddison, PJ *et al.* (2005). Synthetic shRNAs as potent RNAi triggers. *Nat Biotechnol* **23**: 227–231.
10. Fire, A, Xu, S, Montgomery, MK, Kostas, SA, Driver, SE and Mello, CC (1998). Potent and specific genetic interference by double-stranded RNA in Caenorhabditis elegans. *Nature* **391**: 806–811.
11. Park, JE, Heo, I, Tian, Y, Simanshu, DK, Chang, H, Jee, D *et al.* (2011). Dicer recognizes the 5′ end of RNA for efficient and accurate processing. *Nature* **475**: 201–205.
12. Vermeulen, A, Behlen, L, Reynolds, A, Wolfson, A, Marshall, WS, Karpilow, J *et al.* (2005). The contributions of dsRNA structure to Dicer specificity and efficiency. *RNA* **11**: 674–682.
13. Zhang, X and Zeng, Y (2010). The terminal loop region controls microRNA processing by Drosha and Dicer. *Nucleic Acids Res* **38**: 7689–7697.
14. Gu, S, Jin, L, Zhang, F, Huang, Y, Grimm, D, Rossi, JJ *et al.* (2011). Thermodynamic stability of small hairpin RNAs highly influences the loading process of different mammalian Argonautes. *Proc Natl Acad Sci USA* **108**: 9208–9213.
15. Bish, LT, Sleeper, MM, Reynolds, C, Gazzara, J, Withnall, E, Singletary, GE *et al.* (2011). Cardiac gene transfer of short hairpin RNA directed against phospholamban effectively knocks down gene expression but causes cellular toxicity in canines. *Hum Gene Ther* **22**: 969–977.
16. Borel, F, van Logtenstein, R, Koornneef, A, Maczuga, P, Ritsema, T, Petry, H *et al.* (2011). *In vivo* knock-down of multidrug resistance transporters ABCC1 and ABCC2 by AAV-delivered shRNAs and by artificial miRNAs. *J RNAi Gene Silencing* **7**: 434–442.
17. Grimm, D, Streetz, KL, Jopling, CL, Storm, TA, Pandey, K, Davis, CR *et al.* (2006). Fatality in mice due to oversaturation of cellular microRNA/short hairpin RNA pathways. *Nature* **441**: 537–541.
18. McBride, JL, Boudreau, RL, Harper, SQ, Staber, PD, Monteys, AM, Martins, I *et al.* (2008). Artificial miRNAs mitigate shRNA-mediated toxicity in the brain: implications for the therapeutic development of RNAi. *Proc Natl Acad Sci USA* **105**: 5868–5873.
19. Castanotto, D, Sakurai, K, Lingeman, R, Li, H, Shively, L, Aagaard, L *et al.* (2007). Combinatorial delivery of small interfering RNAs reduces RNAi efficacy by selective incorporation into RISC. *Nucleic Acids Res* **35**: 5154–5164.
20. Liu, YP, Haasnoot, J, ter Brake, O, Berkhout, B and Konstantinova, P (2008). Inhibition of HIV-1 by multiple siRNAs expressed from a single microRNA polycistron. *Nucleic Acids Res* **36**: 2811–2824.
21. Boudreau, RL, Martins, I and Davidson, BL (2009). Artificial microRNAs as siRNA shuttles: improved safety as compared to shRNAs *in vitro* and in vivo. *Mol Ther* **17**: 169–175.
22. Boudreau, RL, Monteys, AM and Davidson, BL (2008). Minimizing variables among hairpin-based RNAi vectors reveals the potency of shRNAs. *RNA* **14**: 1834–1844.
23. Giering, JC, Grimm, D, Storm, TA and Kay, MA (2008). Expression of shRNA from a tissue-specific pol II promoter is an effective and safe RNAi therapeutic. *Mol Ther* **16**: 1630–1636.
24. Song, J, Pang, S, Lu, Y, Yokoyama, KK, Zheng, JY and Chiu, R (2004). Gene silencing in androgen-responsive prostate cancer cells from the tissue-specific prostate-specific antigen promoter. *Cancer Res* **64**: 7661–7663.
25. Aagaard, L, Amarzguioui, M, Sun, G, Santos, LC, Ehsani, A, Prydz, H *et al.* (2007). A facile lentiviral vector system for expression of doxycycline-inducible shRNAs: knockdown of the pre-miRNA processing enzyme Drosha. *Mol Ther* **15**: 938–945.
26. Kappel, S, Matthess, Y, Zimmer, B, Kaufmann, M and Strebhardt, K (2006). Tumor inhibition by genomically integrated inducible RNAi-cassettes. *Nucleic Acids Res* **34**: 4527–4536.
27. McJunkin, K, Mazurek, A, Premsrirut, PK, Zuber, J, Dow, LE, Simon, J *et al.* (2011). Reversible suppression of an essential gene in adult mice using transgenic RNA interference. *Proc Natl Acad Sci USA* **108**: 7113–7118.
28. Premsrirut, PK, Dow, LE, Kim, SY, Camiolo, M, Malone, CD, Miething, C *et al.* (2011). A rapid and scalable system for studying gene function in mice using conditional RNA interference. *Cell* **145**: 145–158.
29. Rangasamy, D, Tremethick, DJ and Greaves, IK (2008). Gene knockdown by ecdysone-based inducible RNAi in stable mammalian cell lines. *Nat Protoc* **3**: 79–88.
30. McQueen, MJ, Hawken, S, Wang, X, Ounpuu, S, Sniderman, A, Probstfield, J *et al.*; INTERHEART study investigators. (2008). Lipids, lipoproteins, and apolipoproteins as risk markers of myocardial infarction in 52 countries (the INTERHEART study): a case-control study. *Lancet* **372**: 224–233.
31. Crooke, RM, Graham, MJ, Lemonidis, KM, Whipple, CP, Koo, S and Perera, RJ (2005). An apolipoprotein B antisense oligonucleotide lowers LDL cholesterol in hyperlipidemic mice without causing hepatic steatosis. *J Lipid Res* **46**: 872–884.
32. Zimmermann, TS, Lee, AC, Akinc, A, Bramlage, B, Bumcrot, D, Fedoruk, MN *et al.* (2006). RNAi-mediated gene silencing in non-human primates. *Nature* **441**: 111–114.
33. Koornneef, A, Maczuga, P, van Logtenstein, R, Borel, F, Blits, B, Ritsema, T *et al.* (2011). Apolipoprotein B knockdown by AAV-delivered shRNA lowers plasma cholesterol in mice. *Mol Ther* **19**: 731–740.
34. Miao, CH, Ohashi, K, Patijn, GA, Meuse, L, Ye, X, Thompson, AR *et al.* (2000). Inclusion of the hepatic locus control region, an intron, and untranslated region increases and stabilizes hepatic factor IX gene expression *in vivo* but not *in vitro*. *Mol Ther* **1**: 522–532.
35. Grimm, D (2009). Small silencing RNAs: state-of-the-art. *Adv Drug Deliv Rev* **61**: 672–703.
36. Braglia, P, Percudani, R and Dieci, G (2005). Sequence context effects on oligo(dT) termination signal recognition by Saccharomyces cerevisiae RNA polymerase III. *J Biol Chem* **280**: 19551–19562.
37. Aagaard, LA, Zhang, J, von Eije, KJ, Li, H, Saetrom, P, Amarzguioui, M *et al.* (2008). Engineering and optimization of the miR-106b cluster for ectopic expression of multiplexed anti-HIV RNAs. *Gene Ther* **15**: 1536–1549.
38. Ehsani, A, Saetrom, P, Zhang, J, Alluin, J, Li, H, Snøve, O Jr *et al.* (2010). Rational design of micro-RNA-like bifunctional siRNAs targeting HIV and the HIV coreceptor CCR5. *Mol Ther* **18**: 796–802.
39. Ely, A, Naidoo, T and Arbuthnot, P (2009). Efficient silencing of gene expression with modular trimeric Pol II expression cassettes comprising microRNA shuttles. *Nucleic Acids Res* **37**: e91.
40. Li, C, Xiao, P, Gray, SJ, Weinberg, MS and Samulski, RJ (2011). Combination therapy utilizing shRNA knockdown and an optimized resistant transgene for rescue of diseases caused by misfolded proteins. *Proc Natl Acad Sci USA* **108**: 14258–14263.
41. Mueller, C, Tang, Q, Gruntman, A, Blomenkamp, K, Teckman, J, Song, L *et al.* (2012). Sustained miRNA-mediated knockdown of mutant AAT with simultaneous augmentation of wild-type AAT has minimal effect on global liver miRNA profiles. *Mol Ther* **20**: 590–600.
42. Ely, A, Naidoo, T and Arbuthnot, P (2009). Efficient silencing of gene expression with modular trimeric Pol II expression cassettes comprising microRNA shuttles. *Nucl Acids Res* **37**: e91.
43. Cuccato, G, Polynikis, A, Siciliano, V, Graziano, M, di Bernardo, M and di Bernardo, D (2011). Modeling RNA interference in mammalian cells. *BMC Syst Biol* **5**: 19.
44. Jackson, AL, Burchard, J, Schelter, J, Chau, BN, Cleary, M, Lim, L *et al.* (2006). Widespread siRNA "off-target" transcript silencing mediated by seed region sequence complementarity. *RNA* **12**: 1179–1187.
45. Vandenberghe, LH and Wilson, JM (2007). AAV as an immunogen. *Curr Gene Ther* **7**: 325–333.
46. Livak, KJ and Schmittgen, TD (2001). Analysis of relative gene expression data using real-time quantitative PCR and the 2(-Delta Delta C(T)) Method. *Methods* **25**: 402–408.
47. Chen, C, Ridzon, DA, Broomer, AJ, Zhou, Z, Lee, DH, Nguyen, JT *et al.* (2005). Real-time quantification of microRNAs by stem-loop RT-PCR. *Nucleic Acids Res* **33**: e179.
48. Motameny, S, Wolters, S, Nürnberg, P and Schumacher, B (2010). Next generation sequencing of miRNAs - strategies, resources and methods. *Genes* **1**: 70–84.
49. Mortazavi, A, Williams, BA, McCue, K, Schaeffer, L and Wold, B (2008). Mapping and quantifying mammalian transcriptomes by RNA-Seq. *Nat Methods* **5**: 621–628.
50. Edgar, R, Domrachev, M and Lash, AE (2002). Gene Expression Omnibus: NCBI gene expression and hybridization array data repository. *Nucleic Acids Res* **30**: 207–210.
51. Gao, GP, Alvira, MR, Wang, L, Calcedo, R, Johnston, J and Wilson, JM (2002). Novel adeno-associated viruses from rhesus monkeys as vectors for human gene therapy. *Proc Natl Acad Sci USA* **99**: 11854–11859.
52. Ruijter, JM, Thygesen, HH, Schoneveld, OJ, Das, AT, Berkhout, B and Lamers, WH (2006). Factor correction as a tool to eliminate between-session variation in replicate experiments: application to molecular biology and retrovirology. *Retrovirology* **3**: 2.